# Orbital floor repair using patient specific osteoinductive implant made by stereolithography

Guillaume, Olivier; Geven, Mike A.; Varjas, Viktor; Varga, Peter; Gehweiler, Dominic; Stadelmann, Vincent A.; Smidt, Tanja; Zeiter, Stephan; Sprecher, Christoph; Bos, Ruud R. M.

*Published in:*
Biomaterials

*DOI:*
10.1016/j.biomaterials.2019.119721



*Publication date:*
2020

Biomaterials 233 (2020) 119721

Contents lists available at ScienceDirect

Biomaterials

journal homepage: www.elsevier.com/locate/biomaterials

# Orbital floor repair using patient specific osteoinductive implant made by stereolithography

Olivier Guillaume[a], Mike A. Geven[b], Viktor Varjas[a], Peter Varga[a], Dominic Gehweiler[a], Vincent A. Stadelmann[c], Tanja Smidt[a], Stephan Zeiter[a], Christoph Sprecher[a], Ruud R.M. Bos[d], Dirk W. Grijpma[b], Mauro Alini[a], Huipin Yuan[e], Geoff R. Richards[a], Tingting Tang[f], Ling Qin[g], Lai Yuxiao[g], Peng Jiang[h], David Eglin[a,*]

[a] AO Research Institute Davos, Clavadelerstrasse 8, CH 7270, Davos, Switzerland
[b] MIRA Institute for Biomedical Engineering and Technical Medicine, Department of Biomaterials Science and Technology, University of Twente, P.O. Box 217, 7500, AE Enschede, the Netherlands
[c] SCANCO Medical AG, Fabrikweg 2, CH 8306, Bruettisellen, Switzerland
[d] University Medical Center Groningen, Groningen, the Netherlands
[e] - Xpand Biotechnology BV, Professor Bronkhorstlaan 10-d, 3723, MB Bilthoven, the Netherlands
[f] Shanghai Key Laboratory of Orthopaedic Implants, Department of Orthopaedic Surgery, Shanghai Ninth People's Hospital, Shanghai Jiao Tong University, School of Medicine, Shanghai, China
[g] Innovative Orthopaedic Biomaterial and Drug Translational Research Laboratory of Li Ka Shing Institute of Health, Department of Orthopaedics and Traumatology, The Chinese University of Hong Kong, Hong Kong, China
[h] General Hospital of People's Liberation Army- Beijing 301 Hospital, Beijing, China

ARTICLE INFO

*Keywords:*
Orbital floor
Patient specific implant
Stereolithography
Poly(trimethylene carbonate)
Hydroxyapatite
Sheep model

ABSTRACT

The orbital floor (OF) is an anatomical location in the craniomaxillofacial (CMF) region known to be highly variable in shape and size. When fractured, implants commonly consisting of titanium meshes are customized by plying and crude hand-shaping. Nevertheless, more precise customized synthetic grafts are needed to meticulously reconstruct the patients' OF anatomy with better fidelity. As alternative to titanium mesh implants dedicated to OF repair, we propose a flexible patient-specific implant (PSI) made by stereolithography (SLA), offering a high degree of control over its geometry and architecture. The PSI is made of biodegradable poly (trimethylene carbonate) (PTMC) loaded with 40 wt % of hydroxyapatite (called Osteo-PTMC). In this work, we developed a complete work-flow for the additive manufacturing of PSIs to be used to repair the fractured OF, which is clinically relevant for individualized medicine. This work-flow consists of (i) the surgical planning, (ii) the design of virtual PSIs and (iii) their fabrication by SLA, (iv) the monitoring and (v) the biological evaluation in a preclinical large-animal model. We have found that once implanted, titanium meshes resulted in fibrous tissue encapsulation, whereas Osteo-PMTC resulted in rapid neovascularization and bone morphogenesis, both ectopically and in the OF region, and without the need of additional biotherapeutics such as bone morphogenic proteins. Our study supports the hypothesis that the composite osteoinductive Osteo-PTMC brings advantages compared to standard titanium mesh, by stimulating bone neoformation in the OF defects. PSIs made of Osteo-PTMC represent a significant advancement for patients whereby the anatomical characteristics of the OF defect restrict the utilization of traditional hand-shaped titanium mesh.We propose a work-flow to design and fabricate biodegradable and bone-promotive patient specific implants to be used in craniomaxillofacial surgery for bone reconstruction.

## 1. Introduction

The human orbit markedly varies in shape, size and geometry as other bony structures in the craniomaxillofacial (CMF) region. In case of fracture, the biggest challenge for the surgeon is the availability of implants with a good fit with the patient specific anatomical features. In fact, a mismatch between the implant geometry and the patient anatomical structures can result in a misalignment of the orbit with the

* Corresponding author.
*E-mail address:* david.eglin@aofoundation.org (D. Eglin).

https://doi.org/10.1016/j.biomaterials.2019.119721
Received 31 July 2019; Received in revised form 20 December 2019; Accepted 20 December 2019
Available online 23 December 2019
0142-9612/ 

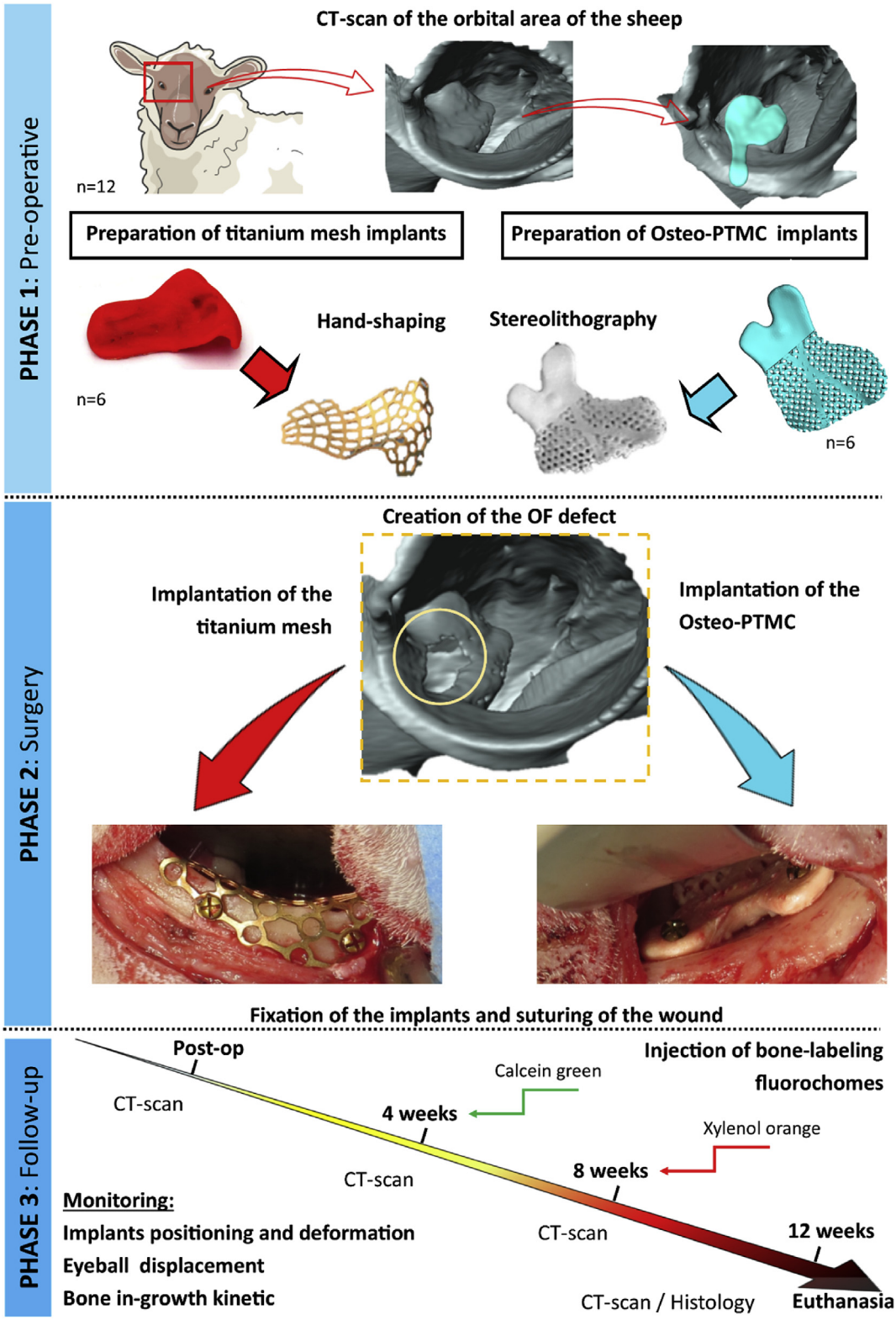


**Fig. 1.** General work-flow and study design.

severe consequence of loss of vision for the patient. The anatomical specificities of the CMF region have motivated researchers and clinicians to create implants with customized features to restore normal orbit anatomy and function [1]. Pre-operative facial CT scan of patients affected by CMF fractures are routinely conducted to evaluate the degree of tissue damage and to perform a pre-operative surgical planning [2,3]. CT scans are also used to design and to print plastic anatomical models employed to manually adapt a standard implant to anatomically reconstruct the patients' fractured bones [4]. Such printed anatomical models are used in the clinic to manually shape orbital floor (OF) implants made of metal alloy [5], titanium [4,6–10], pure polylactic acid (PLA) [11], composites with hydroxyapatite (HA) [12], and even bone grafts [13]. The shaped implants facilitate and shorten the surgical procedure as their geometries do not need to be adjusted manually

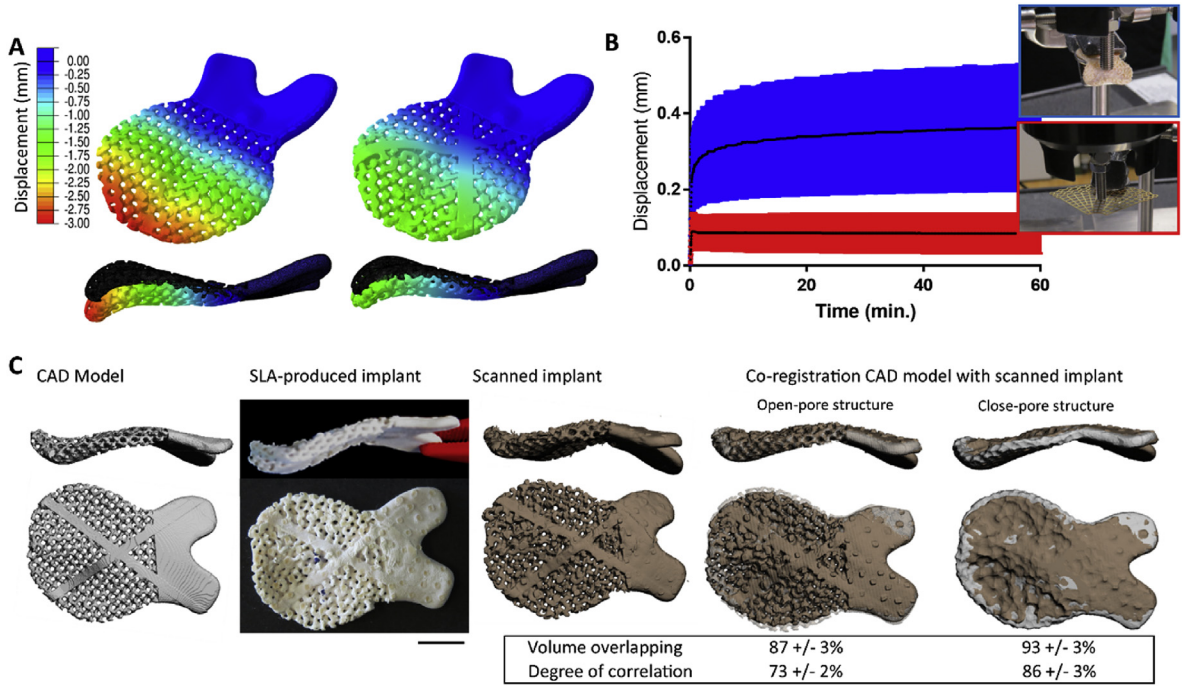


**Fig. 2. Optimization and characterization of the SLA-fabricated PSI.**
Finite Element analyses were conducted on virtual PSIs with different architectures (gyroid-porous PSI non-reinforced (left side) and reinforced (right side)) to monitor implant behaviour under cantilever bending test (**A**). Cantilever mechanical testing of titanium mesh *versus* Osteo-PTMC PSI revealing the different bending properties of the materials (**B**). A quality control process was established in order to assess the feasibility to produce PSIs with accurate and reproducible macroscopic and microscopic features compared to the initial CAD model (**C**).

intra-operatively. Still, improvements can be made by directly fabricating the implants with not only an optimal overall shape factor, but also suitable biomechanics and biofunctionality.

Calcium phosphate ceramics (e.g. hydroxyapatite) are often used as bone void filler in oral surgery (e.g. granules or putty pastes used in dental application) as they are biocompatible, osteoconductive, and can be placed manually to fill bone defects [14,15]. Nevertheless, their mechanical brittleness and the impossibility for direct implant fabrication limit their use in personalized medicine (i.e. post-printing debinding and sintering would be needed for the fabrication of strong calcium phosphate ceramic implants). Another important limitation is that very few available ceramic-based bone substitutes are shown to possess truly osteoinductive properties [16]. Conversely, PSIs made from titanium have been reported for OF, but titanium is non-degradable and most often bioinert. Synthetic thermoplastic polymer-based implants (e.g. polylactic acid) allow for direct fabrication of implants, but such biomaterials are not bioactive. The introduction of HA inside biodegradable polymeric matrices improves the bioactivity of the implants and could even endow the composite biomaterials with osteoinductivity [17]. However, the osteoinductive properties were shown to vary largely with the polymers' composition [18] and the bulk degradation of such composites is far from optimal for an appropriate osseointegration. Indeed, long-term *in vivo* study showed that PLA-based implant degradation triggers exacerbated osteolytic reaction along with an intense inflammatory response [19].

As alternative material to polyesters, laminate structures of poly (trimethylene carbonate) (PTMC) loaded with biphasic calcium phosphate particles have been fabricated using compression molding. Those structures showed the ability to promote the repair of fractured OF in a sheep model [20]. Indeed, it was shown that PTMC/CaP composites exhibit interesting features in terms of degradation mechanism through enzyme-mediated surface erosion [21–23], protein adsorption and calcium release [24], which promote bone formation. Nevertheless, the selected fabrication technique, i.e. compression molding [20], was not suitable to develop an implant with customized PSI features and appropriate osseointegration.

There is a global clinical need for biomaterials that can be processed using additive manufacturing in order to produce PSIs endowed with osteogenic activity while being degradable. In this work, we proposed a novel type of PSI which is manufactured by stereolithography (SLA). This type of implant enables the production of customized structures that maintain the position of the orbit similarly to the standard hand-plied titanium implants, but actively promote bone formation in OF defects thanks to its biodegradable and osteogenic components (*i.e.* poly(trimethylene carbonate) with 40 wt% HA, called Osteo-PTMC). The full process including the pre-operative surgical planning, virtual implant design and optimization, SLA-fabrication, quality control along with post-operative monitoring and biological response was conducted in a large animal model with OF fracture. The overall functionality and biological response of the Osteo-PTMC implants are compared to the clinical standard hand-shaped titanium meshes. This work represents an unprecedented proof-of-concept for the whole fabrication chart for PSIs dedicated to high-fidelity OF repair and beyond.

## 2. Results

### 2.1. Experimental design of the study

Pre-operatively, the of the sheep (only right orbital, n = 12) were scanned and virtual PSIs were designed using an image processing software to entirely cover the region of the OFFig. 1). The corresponding STL. files were obtained and used either to print plastic molds via Fused Filament Fabrication (FFF) for hand-shaping of titanium meshes or to design porous PSIs and to subsequently produce Osteo-PTMC implants via SLA. During the surgery, the OF were resected (only right orbital) and covered by either the titanium mesh or the PSI made of Osteo-PTMC (n = 6/group), stabilized in the infraorbital rim by 2 titanium screws. Post-operatively, the OF area of every sheep was repeatedly CT-scanned to measure PSIs functionality, i.e. implant positioning, eyeball displacement and osteogenic activity. In addition, the

bone ingrowth kinetics was assessed by two longitudinal fluorochrome injections. The animals were euthanized at 12 weeks post-operatively, and samples were analyzed for bone formation and osseointegration (by CT-scan and histology).

### 2.2. Design and SLA-fabrication of personalized implants

The effect of the PSI implant architecture of the pores (triply periodic minimal surfaces: IWP, diamond and gyroid), the thickness of the strut and the volume of porosity along with reinforcement design were investigated by means of finite element (FE) simulations. The simulations indicated that, using gyroid pore design with the cross-shaped reinforcing structure increased the structural stiffness by 75%, in a loading mode mimicking the experimental cantilever bending setup (applying clinically relevant forces, *i.e.* 0.3 N in the center of the structure [25], Fig. 2A, Movie S1). The structural stiffness results for the original and the cross-reinforced models were 0.270 and 0.472 N/mm, respectively. From this observation, we decided to confer this cross-shaped reinforcement design to all the SLA-produced PSIs to make them less prone to deformation. The versatility of this approach is shown in SD 2, where the effect of the other tested PSI architectural features, including the pores, the thickness of the struts and the volume of porosity along with other reinforcement designs are presented.

Supplementary data related to this article can be found at https://doi.org/10.1016/j.biomaterials.2019.119721.

We then investigated experimentally the PSI mechanical behaviour in anatomically relevant scenarios, such as those experienced in the human orbital region [25]. The cantilever set-up used was a worst-case scenario, which would correspond clinically to a complete OF resection, without any further bony parts physically supporting the implant in the posterior part of the orbital. In such configuration, the main physical stabilization originates from the fixation area where the two screws are inserted in the infraorbital buttress. The uniaxial cantilever mechanical test revealed that the PSI made of Osteo-PTMC is less stiff than the titanium mesh, with an average displacement measured in the middle of the specimen of 0.38 mm and 0.10 mm respectively (Fig. 2B).

A quality control process was established to verify the degree of accuracy of the SLA-fabrication. PSIs were produced using SLA and co-registered with their initial virtual implants originating from the CT-scans (CAD model, Fig. 2C). Depending on the scale of interest, from micrometric details (open-pore structure) to larger macrometric general shapes (closed-pore structure), the degree and volume of correlation differed, but were always close to the designed models. The larger differences observed on the microscale details of the open-pore structures are due to the limitations of the SLA resolution when printing viscous composite resins. The necessity to have supportive pillars to prevent PSIs to collapse during the fabrication and their subsequent manual cut changes locally the surface topography and its chemical composition (in terms of Ca and P, SD 3). Optimization of those pillars arrangement and location can be implemented in the work-flow to minimize their potential effect on the bone-implant integration.

### 2.3. In vivo monitoring of PSIs functionality

Pre-operatively, implants including hand-shaped titanium meshes (n = 6) and SLA-fabricated Osteo-PTMC (n = 6) were designed and fabricated (all the implants are shown SD 4). As the OF in sheep varies markedly in shape and size, pre-operative CT scanning was necessary for both groups, to either print Osteo-PTMCs or to shape titanium meshes. The high specimen variability regarding the surface of the OF to be covered by the implants (SD 4) clearly supports the necessity to develop an individualized implant design strategy. Thus, the 12 sheep were pooled in the two distinct groups in a way that the average surface of the materials to be implanted was not significantly different. The surgical act was simplified by the fact that the implants of both groups have been tailored to fit the OF shape and surface. The surgical procedure with defect creation and reconstruction of the orbital floor with either a pre-bent titanium mesh or the custom-made SLA printed Osteo-PTMC was well tolerated by all 12 sheep. There was a mild to moderate swelling around the surgical wound and lower eyelid during the first week after surgery, which disappeared without further treatment. One sheep (specimen *a4*) had a wound dehiscence. Following debridement, re-suturing was necessary after which healing proceeded uneventful. For this animal, antibiotic administration was extended for 5 days (Ceftiofur 2.2 mg/kg BW, s.c.). Clinically there was no difference between the two groups, bulbus movement or position did not change from before to after surgery and during the whole study period. One sheep (specimen *a6*) gave birth to one lamb 14 days after surgery, even though she did not develop a milk producing udder or showed any other signs of pregnancy.

No implant failure (SD 5) and no major misplacement were observed post-operatively between the surgical plan and the implantation (implanted materials on the OF region are shown (Movies S2 and S3) for titanium (specimen *a3*) and Osteo-PTMC (specimen *b2*) respectively). The radiographic time-lapse scans permitted to easily localize, control and monitor the stability and displacement for both titanium mesh and Osteo-PTMC implants (examples are shown in Fig. 3 A-D and SD 6). Implants were adequately positioned, except for the PSI made of Osteo-PTMC number *b3*, where a slightly more frontal position was observed (SD 6).

Supplementary data related to this article can be found at https://doi.org/10.1016/j.biomaterials.2019.119721.

The follow-up did not reveal any signs of implant deterioration or failure. We observed and quantified implants deformation occurring locally over time (illustrated for titanium meshes in Fig. 3E and for Osteo-PTMC in Fig. 3F). Low displacement (in this case bending) was observed for titanium mesh (comprised between 0.3 and 0.6 mm), except for one specimen (titanium mesh *a1*) where a 1.8 mm bending was noted probably due to the slight initial mis-positioning during the surgery (reported in SD 6). Globally, higher bending was observed for PSIs made of Osteo-PTMC compared to titanium meshes, with average values ranging from 0.6 to 0.9 mm (a maximal implant bending was registered for specimen *b5*, with a 1.5–1.8 mm displacement). The differences observed between both groups of implants correlate with the mechanical testing results presented in Fig. 2C, with titanium mesh being significantly stiffer than Osteo-PTMC implant. The eyeball displacement assessed by CT scans (illustrated Fig. 3G), demonstrated two different tendencies depending on the type of implant. The implantation of titanium mesh was responsible for a dorsal displacement of the sheep eyeball (in 4 out of 6 specimens, Fig. 3H). *A contrario*, PSI implants made of Osteo-PTMC triggered post-operatively a ventral displacement of the eyeball, which became more pronounced over time (in 5 out of 6 specimens, Fig. 3H). Nevertheless, for both materials, the displacement tendencies are minor (less than 1 mm), which can explain the fact that no signs of vision problems or mis-aligned eyeballs could be detected on any animals.

### 2.4. Investigation of PTMC-based implants biocompatibility

Histological assessment of the PTMC-based materials biocompatibility compared to the Ceramics implanted IM after 3 months is presented Fig. 4. PTMC implants were covered by a fibrous scare tissue, elicited a very low grade of granulomatous inflammation and almost no granulocytic and lymphocytic reaction (Fig. 4A). In the Osteo-PTMC implants, an increased inflammatory reaction with higher number of foreign body cells was observed (Fig. 4B), which was similar to the marked inflammatory reaction with presence of multinucleated foreign cells observed on the surface and interstitium of the Ceramic implants (Fig. 4C).

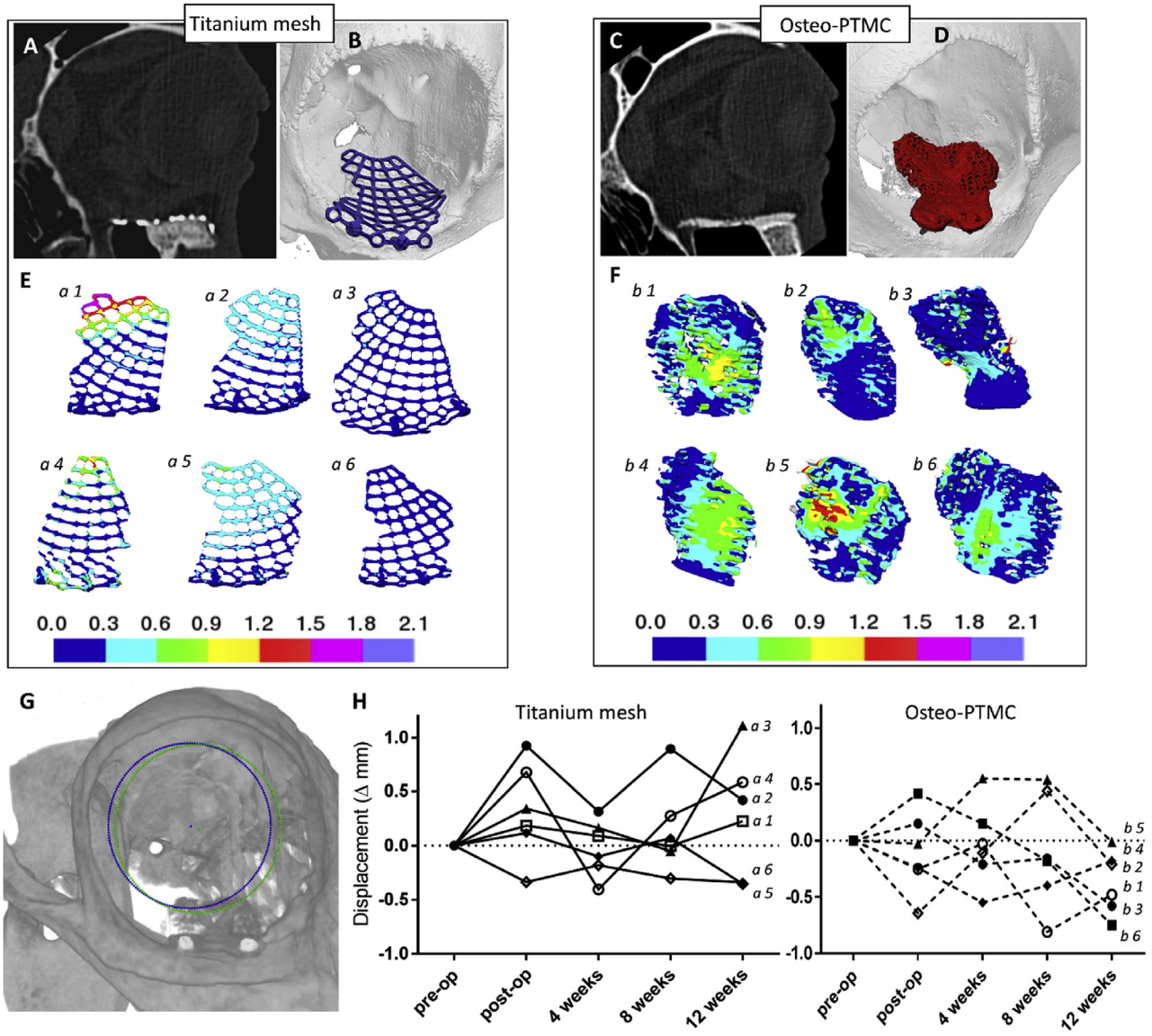


**Fig. 3. Post-operative functionality and behaviour of different implants in the OF region.**
12 weeks post-operative appreciation by clinical CT acquisition and 3-Dimensional reconstruction using HR-pQCT (SCANCO Medical AG, Switzerland) of titanium mesh (**A** and **B**) and of PSI made of Osteo-PTMC (**C** and **D**). Monitoring of the implant displacement (post-op day 1 *versus* week 12, coloured-scale in mm) of the titanium meshes (**E**) and of the PSIs made of Osteo-PTMC (**F**). Eyeball displacement assessment (illustrated in **G**, with blue and green circles representing post-op day 1 *versus* week 12 respectively) and chronological quantification for titanium meshes and Osteo-PTMC implants (**H**).

### *2.5. In vivo bone forming assessment*

We have recently evaluated the regenerative potential of the Osteo-PTMC in a rabbit calvarial defect model [24]. In this new investigation, we aimed at validating the utilization of the same biomaterials as a PSI to support bone formation in OF fracture in a larger animal model.

The deposition of mineralized tissue in Osteo-PTMC implants was monitored radiographically (Fig. 5A and B), revealing longitudinal bone ingrowth for all six PSIs. Differences in terms of bone healing kinetic could be detected between specimen *b1, b2* and *b4* for which the bone growth slowed-down 1-month post-surgery. In comparison, for the specimen *b3, b5* and *b6*, a continuous bone deposition could be observed over the 3-month experimentation. Such assessment was not possible on the titanium mesh due to its strong artefact signal using conventional clinical CT. Further analyses were conducted using a high-resolution prototype microCT 100, revealing the absence of new bone formation between the struts of all the titanium mesh implants (Fig. 5C).

Investigation of bone morphogenesis using histological staining confirmed the radiographic outcomes (Fig. 6). Indeed, there was no sign of direct bone integration with the titanium mesh implants (Fig. 6A and B). The titanium mesh filaments were encapsulated in a fibrous tissue rich in aligned fibers of collagen; in some locations, only an indirect contact with bone tissue was observed (Fig. 6C). In the latter case, it is interesting to note that there was always a gap of few hundred micrometers between the bone and the surface of the implant composed of fibrous tissue with presence of inflammatory cells such as macrophages, signature of a poor implant osseointegration.

The sequential fluorochrome staining demonstrated that the bone was formed from the surface of the old bone, growing toward the titanium mesh, which is a characteristic of a distance osteogenesis mechanism (Fig. 6D). In opposition, an excellent osseointegration was observed for the implants made of Osteo-PTMC, with bone formed mainly at the basal surface of the implant (where the former OF bone was located before its resection, illustrated Fig. 6E). A direct bone-to-implant contact was observed at numerous areas, ensuring a good

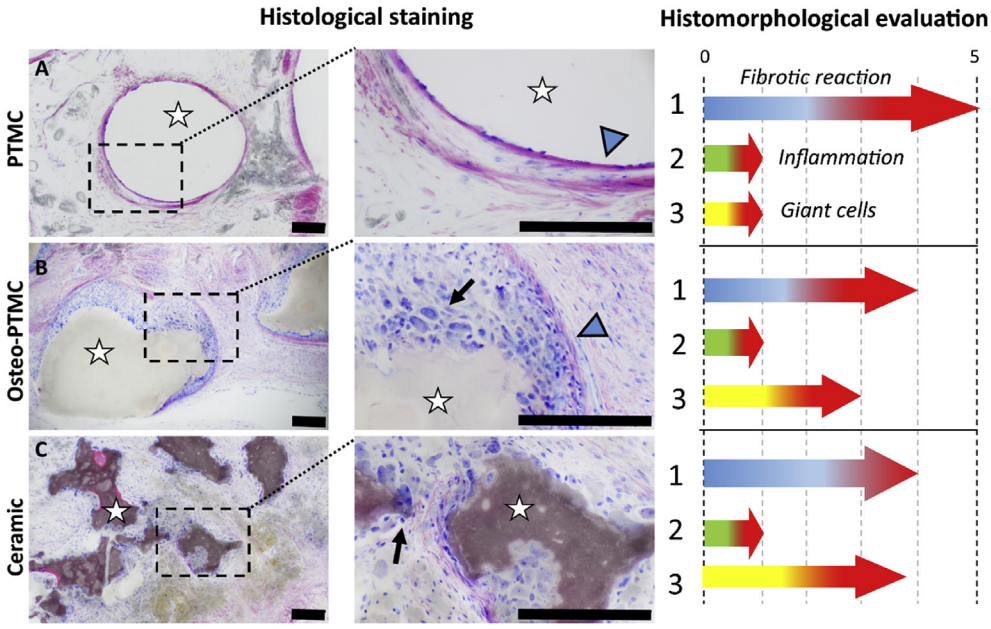


**Fig. 4. Biocompatibility of PTMC-based biomaterials compared to Ceramic in intra-muscular site.**
**Histological staining** of the neo-formed tissue invading the porosity of the different biomaterials 3 months after implantation intra-muscularly (PTMC, Osteo-PTMC and Ceramic are shown pictures **A, B** and **C** respectively). The materials cross-section is denoted with the white stars and the scale bars represent 200 μm. Blue head-arrows illustrate the surface materials in contact with fibrous encapsulation and the black arrows denote the giant cells. **Semi-quantitative histomorphological evaluation** was conducted by an anatomopathologist taking into consideration the intensity of 1- the fibrotic reaction and the thickness of fibrous encapsulation of the materials, 2- the inflammation with the granulocytic/lymphocytic reaction, and 3- the presence of foreign body giant multinucleated cells. Grading scores ranged from 0 (absence) to 5 (high).

stabilization of the implant in this surgical site (Fig. 6F). The fluorochrome injections revealed that the surface of the Osteo-PTMC itself stimulated bone formation, with bone growing from the surface of the materials toward the porous compartment, which is characteristic of a contact osteogenesis mechanism (Fig. 6G). The non-operated sham group is shown as reference (Fig. 6H), where the organized bone architecture of the OF with osteoclasts laying in between the bone lamellar structure can be appreciated (Fig. 6I). The presence of the two

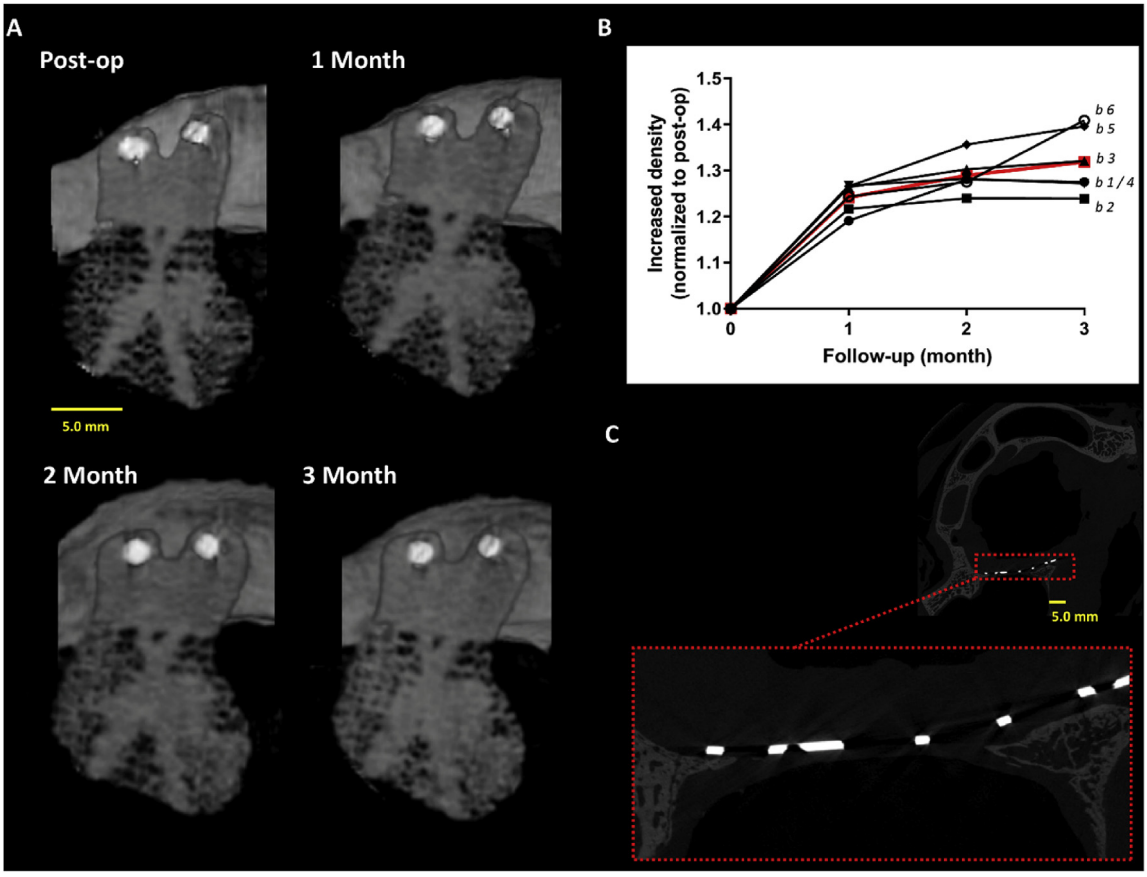


**Fig. 5. Monitoring neo-bone formation using time-lapse CT scans.**
Example of time-lapse CT scans of Osteo-PTMC implant illustrating the area of mineralization increasing over time through the porous network (**A**), and longitudinal quantification of the evolution of Osteo-PTMC implants' radiodensity, corresponding to mineralization (**B**, the average trend is shown with the red line). Such analysis was not possible on titanium mesh due to the resulting high artefact signal. Nevertheless, a post-euthanasia investigation using high resolution microCT 100 did not show any new bone formation for this group (**C**).

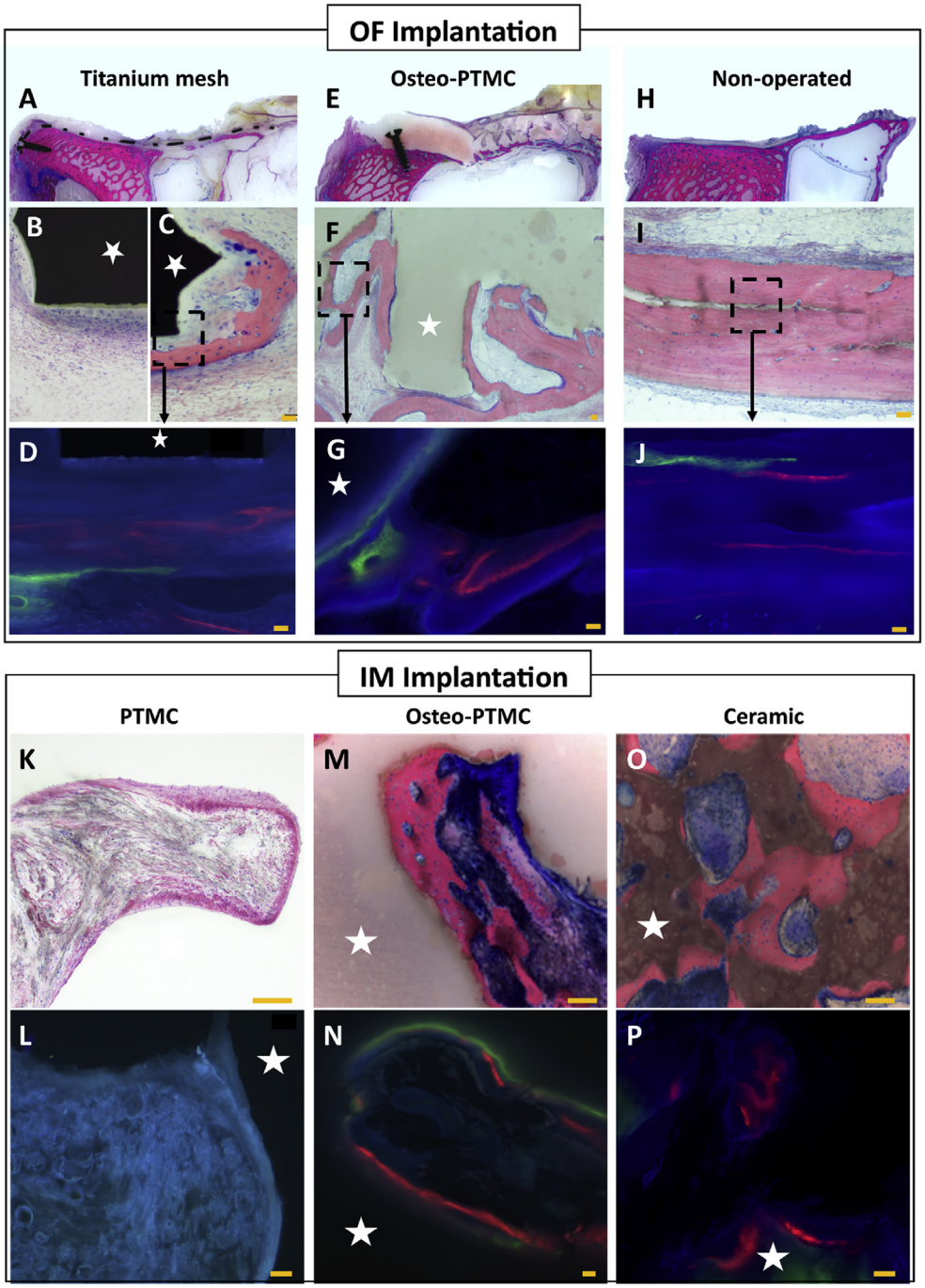


**Fig. 6. Histological evaluation of bone remodelling in two anatomical sites.**
**Orbital region**: Bone regeneration assessed by histological staining and fluorochrome detection after a 12-week implantation of titanium mesh (**A**, **B**, **C** and **D**) and Osteo-PTMC (**E**, **F** and **G**). Non-operated OF bone is shown as control (**H**, **I** and **J**). Calcein green and Xylenol orange stained new bone formed at 4 and 8 weeks respectively.

fluorochromes revealed a constant remodelling of the OF bone even in the non-operated OF (Fig. 6J). The thickness of the fluorescent tissue layers and their inter-distance observed was smaller in this group, compared to the two other operated groups (Fig. 6D and G), indicating that bone turn-over in the sham group is less intense and slower than in the operated groups. Other representative panoramic histological cross-sections of the three groups are shown in SD 7.

**Intra-muscular region**: Ectopic bone formation detected by histological staining and fluorochrome detection after a 12-week implantation of PTMC (**K** and **L**), Osteo-PTMC (**M** and **N**) and osteoinductive ceramic (**O** and **P**). The materials cross-section is denoted with the white stars and the scale bars represent 50 μm. Mesenchymal collagenous condensation appears as a blue staining on the images (**M** and **O)**.

Finally, to further assess the biological functionality of the Osteo-PTMC materials, plugs of equal composition to the PSIs were implanted in non-bony sites (IM), and the neo-bone formation was compared to negative control materials, plugs of photo-cured PTMC without HA, and to positive controls (i.e. osteoinductive ceramic plugs). Histologically, we observed striking differences in terms of biological response of PTMC compared to Osteo-PTMC. Only soft tissue containing mature collagen fibers, with relatively low cellular density was seen in PTMC

plugs (Fig. 6K and L). In comparison, Osteo-PTMC triggered bone formation in this ectopic site (in 7 out of 12 specimens), validating that this composition is not only osteoconductive [24], but exhibits also as a certain degree of osteoinductivity (Fig. 6M and N). However, this observation was not systematic, and in the other 5 specimens, the biological response was similar to PTMC only, with soft fibrous tissue penetrating the porous network of the materials (SD 8). The osteoinductivity of the ceramic materials was also validated in this model [26], and intense bone formation, presence of mesenchymal collagenous tissue and high cellular density penetrating the porous network were observed (Fig. 6O and P). The fluorochromes staining showed that the front of bone was in majority formed after 8 weeks of implantation (red fluorescence) for both Ceramic and Osteo-PTMC materials (Fig. 6N). No fluorescent staining could be detected for PTMC (Fig. 6L) validating the lack of osteogenicity of PTMC alone.

In comparison to the orbital site where new bone formation could be detected after only 4 weeks of surgery, this ectopic site required a longer activation period to permit recruitment of progenitor cells and bone formation. On both Ceramic and Osteo-PTMC, an intense bone remodelling was detected, with presence of osteoclasts embedded in bone lacuna, layers of osteoblasts depositing new bone on top of the existing ones, neovascularization penetrating the porous network. Signs of material degradation such as eroded surfaces and cracks could be observed as well as presence of giant multinucleated cells (illustrated Fig. 4 and SD 9).

## 3. Discussion

### 3.1. Designing implants with high degree of personalization

The rapid growth of 3D modelling and printing technologies are revolutionizing numerous surgical fields, with cranioplasty being one of the most important beneficiaries [27]. Indeed, radiologists routinely conduct facial CT scan to evaluate the degree of tissue damage, to perform virtual pre-operative surgical planning or to print plastic anatomical models employed to manually adapt the implant to the shape of the orbital region of the patient. There are only few examples of custom-made titanium implants directly printed and applied in clinics to better accommodate challenging OF surgical defects [9,10,28], while the vast majority of implants have standard geometries and need to be crudely hand-shaped and cut using pliers to achieve optimal positioning.

The establishment of a complete work-flow is crucial for the development of PSIs. Here, we established a complete work-flow from clinical CT scans, to pre-operative design of virtual implants, to optimization of their geometry, mechanics and biological response depending on the defect characteristics, to the production of PSIs using stereolithography and to the monitoring of the post-operative functionality. If required, the principle of mirroring symmetry can easily be implemented in clinics using the non-affected orbit as a template to the proposed chart [28].

In combination with FE modelling, we demonstrated as a proof-of-concept that the mechanical behaviour of the implants is directly influenced by changes in the configuration of the inner and outer structure of the PSI, by variations in the pore volume and geometry and by the integration of dense cross-element reinforcing structures (SD 2). Such type of FE modelling represents an additional digital tool in the armamentarium of the surgeons to further customize and virtually plan the features of the PSI, depending on the geometric and mechanical specificity of the anatomical defects. Offering such *in silico* testing platform is of paramount importance, as inappropriate medical device design is still one of the main reasons of 3D-printed implant post-operative complications [29].

Among the available AM technologies, SLA was selected as it allows *i)* to achieve structures with high degree of complexity and precision [27,30,31], and *ii)* to process viscous biphasic resins required to fabricate Osteo-PTMC-based materials. An important requirement in the production of anatomically-accurate materials is the match between the virtually designed implant and the fabricated equivalent. Indeed, misfitting PSIs can clinically be responsible to visual disturbance and unsatisfying aesthetic outcomes [32]. A quality control (QC) process was developed, that permits to image, to superimpose and to quantify the degree of similarity between the planned and fabricated PSI (Fig. 2). Such QC can be integrated in the chart of fabrication to accept or exclude a fabricated PSI depending on predefined threshold values.

Similarly to the human condition, the heterogeneity of the OF regions in this sheep model in terms of shape and surface observed (SD 4), along with the diversity in the types of fractures, justify the need to develop implants with individualized features [33]. We fabricated PSIs designed to enable a stable anchorage over the infraorbital rim (thanks to the overhanging “fish-tail” ledge), have an optimal fitting to the OF cavity of the sheep and provide an optimized internal architecture and composition for improved mechanical stability, integration and repair.

A perspective of such study would be not only to adapt the shape of the PSI to the surgical site as it is done here, but additionally its mechanical competence. Longitudinal CT scans permitted to appreciate the final positioning of the implants based on the pre-operative initial plan (SD 6), thanks to the radiopacity of the Osteo-PTMC. This monitoring step indicated that the majority of the implants were correctly positioned, and we decided not to retrieve the specimen slightly misplaced (i.e. Osteo-PTMC *b3*) due to the high healthcare burden for the animal, even though such procedure could be envisioned clinically in a computer-assisted surgical act.

The preclinical investigation confirmed that titanium meshes, due to their inherent stiffness, are stable over the maxillary sinus (bending of titanium mesh inferior to 0.6 mm was recorded over time, Fig. 3). In comparison, Osteo-PTMC are less rigid (as shown Fig. 2), and tend to sink slightly more in the cavity formed after resecting the OF (Fig. 3). Nonetheless, it is worth noting that there was no direct correlation between the degree of Osteo-PTMC implant deformation and the eyeball displacement (Fig. 3H). The implant characterized with the highest degree of deformation (specimen *b5*, Fig. 3F) corresponds to the lowest degree of eyeball displacement (Fig. 3G). If the orbital volume is not satisfyingly restored and/or the implant inappropriately positioned, long-term complications might happen, including persistent diplopia (double vision), enophthalmos (posterior displacement of the eyeball within the orbit), ocular movement limitation and even visual loss [34–36]. This sheep model has been successfully introduced to study the suitability of novel material implants to repair OF [20,37,38], as its orbit exhibits similarities to human anatomy, such as a thick infraorbital rim and a very thin floor covering the maxillary sinus. Certainly, one of the limitations of such pre-clinical investigation is the difficulty to record some of the mentioned complications. Nevertheless, following the surgery and during the post-operative period, no physiological signs of any eye-related complications could be detected by the veterinarians. The eye displacement evaluation over time shown in Fig. 3H revealed that titanium meshes tend to trigger slight eye migration dorsally, whereas Osteo-PTMC tends to result in a more ventral eye displacement (toward the maxillary sinus cavity). Those tendencies are not correlated with differences in the thickness of the implanted materials, which is 0.4 mm for titanium mesh and approximately 2.0 mm for Osteo-PTMC. We hypothesized that such differences might be due to either the difference in bending behaviour (Osteo-PTMC being less stiff than titanium mesh, Fig. 2B) or to the biological response to the materials. Indeed, a clear distinction was observed in this 3-month animal study in terms of tissue reaction depending on the nature of the implanted materials. Histologically, we observed that the titanium mesh was not integrated in the underlaying bone but was separated from it, covered by a dense connective tissue capsule (Fig. 6A and SD 7). In contrast, Osteo-PTMC was well stabilized and integrated on its basal part in the bony floor of the orbita (Fig. 6E and SD 7), which might have prevented eyeball bulging. Comparing to the clinical situation, the reported values

in Fig. 3H correspond to insignificant variations. In fact, in humans a measurable difference of up to 2 mm in the relative position of the globes have been reported by normal patients, and the threshold to detect enophthalmos in patients affected by OF fractures lies between 3 and 4 mm [39].

Finally, an important parameter to take into consideration is the possibility to translate our work-flow to the clinical situation in terms of timing. Following a traumatic fracture of the OF and when the surgery is advocated, the recommendation is to operate within 10–14 days to allow for oedema resorption [40,41]. This pre-operative delay period would be then sufficient to integrate the entire work-flow presented in this work to the clinics, including the surgical planning, virtual PSI design, fabrication, QC and sterilization.

### 3.2. PSIs made of Osteo-PTMC regenerate bone in fractured OF

To address the lack of osteopromotive properties of titanium as OF implants, we proposed a novel HA-filled PTMC implant that aims to temporarily support the orbital content and degrade over time while stimulating neo-bone formation.

Even though titanium meshes and polyethylene membranes are amongst the standard materials to fix OF defects due to their stability and bioinert behaviour, it is recognized that the utilization of osteopromotive implants would be beneficial [42,43]. Indeed, the contact area between the fractured margins and the implant is often too limited to allow for an osteogenic cell migration and sufficient neo-bone formation. Our tomography and histological investigations confirmed that there was no direct bone-to-implant contact area detected in the titanium mesh group within the 3 months of the experiment. Indeed, titanium filaments were covered by fibrous tissue rich in collagen fibers and ossification originated only from distance osteogenesis, starting from edge of surrounding original bone (Fig. 6B–D). This fibrotic reaction has been reported to contribute to post-operative complications for the patients when orbital tissues adhere to the implant surface or through its bidimensional porosity [44,45]. In our orbital model, we observed that titanium mesh was responsible for a significant immune reaction with presence of inflammatory cells such as macrophage and encapsulation of the implant inside a fibrous tissue.

For such reasons, synthetic bone promoting implants, based on HA embedded in polymeric structures have been proposed using permanent PE or degradable polyesters (PLLA, PCL) and more recently PTMC [20,42,43]. The rationale is that, by promoting the formation of bone tissue rather than scar tissue in the fractured site, risks of long-term complications can be decreased.

Polyester-based OF implants have been used in clinics, but their efficacy is still controversial, and exaggerated foreign body reaction, inappropriate degradation kinetics and limited bone healing capacity are amongst the limitations frequently reported in the scientific literature [36,37,46,47]. We previously optimized the PTMC composite scaffolds under *in vitro* and *in vivo* situations [24]. Those preliminary data have motivated the selection of PTMC loaded with 40 wt % HA for the OF implant, as no sign of exaggerated inflammatory response was observed, while those materials could promote bone formation [24]. The biocompatibility study resulting from the 3-month IM implantation (Fig. 4) was in agreement with a previous report on PTMC degradation. Rongen et al. demonstrated that during the slow surface-eroding degradation process, the biological tolerance of the photo-crosslinked PTMC implanted subcutaneously was high, with peri-prosthetic tissues similar to the ones observed in our investigation conducted intramuscularly, indicating low degree of inflammatory reaction and fibrous capsule formation [23]. Interestingly, the Osteo-PTMC composition is not only osteoconductive [24], but exhibits also a certain degree of osteoinductivity, as ectopic bone formation was detected in this large animal study (Fig. 6M and N and SD 8). This means that the described Osteo-PTMC exhibits “intrinsic osteoinductivity”, defined as materials being able to drive undifferentiated inducible osteoprogenitor cells toward the osteogenic lineage [48]. To the best of our knowledge, such property has never been reported so far for composite polymer-ceramic scaffolds fabricated using additive manufacturing, but only on salt-leached porous scaffolds [17] or dense granules [18].

We have previously shown that adding 40 wt % of HA into the PTMC matrix is responsible for a significant improvement of the mechanical properties (compared to PTMC or to PTMC with 20 wt% of HA [49]) for a surface-enrichment of HA one more time validated in those PSIs (shown SD 3), for an *in vitro* release of free $Ca^{2+}$ and for a significant protein adsorption [24]. Another important factor which is known to play a key role in bone repair is the surface roughness of the implant, which for the Osteo-PTMC is around 5 times higher than for titanium mesh (Ra of 10.93 *versus* 1.99 μm respectively, SD 3). Those phenomena have been described as being key factors for ceramic-based scaffolds to promote bone formation in orthotopic sites [50]. *A contrario*, the processes involved for material induced-ectopic bone formation are still not entirely elucidated. Until recently, the scientific community agreed on the fact that the release of calcium and phosphate ions from ceramic-based materials, and their subsequent accumulation in supra-physiological concentration, was responsible to the formation of a precipitated biomimetic apatite layer. This layer of apatite formed onto the surface of the implants allows for osteogenic proteins adsorption, which is essential for the recruitment of stem cells and their differentiation towards osteoblastic lineage [50].

Such mechanism cannot explain why some Ca-free materials may also exhibit intrinsic osteoinductivity (e.g. some metals [51] and polymer [52]). This is the reason why a different concept has been recently suggested by Bohner et al. [53], whereby rather than a peri-implant accumulation of the mentioned ions, a depletion of calcium and phosphate due to the formation of an apatite layer may be at the origin of material induced-ectopic bone formation. Along with the formation of this bioactive apatite layer, osteoinductivity also requires a porosity that is suitable for neovascularization and, consequently stem cell recruitment.

This paradigm represents an important shift for the development of osteoinductive materials and motivates further investigations to elucidate why certain biomaterials like the Osteo-PTMC possess this characteristic.

In our experiment, we saw striking differences between scaffolds of similar composition, *i.e.* Osteo-PTMC, in terms of tissue ingrowth and extracellular matrix (ECM) deposition inside their porous network. Indeed, some of the Osteo-PTMC implants did not enable ectopic bone formation, but were filled with a high amount of fibrous collagen that may have impeded progenitor cell migration to the implant surface. On the other hand, the Osteo-PTMC specimens which promoted bone formation were rich in a loser network of ECM which may have acted as temporary template for all the cascade of events necessary for bone formation (SD 8). Indeed, the bone morphogenesis cascade in ectopic sites requires first a suitable porous structure which allows for mesenchymal tissue condensation [54]. This mesenchymal collagenous condensation preferentially initiates at the surface of specific topographic features, *i.e.* within concavities such as the gyroid architecture [54], which corroborates our findings shown SD 8D and E.

In the orbital region, the PSIs made of Osteo-PTMC allowed for rapid bone formation (i.e. already within the first month of implantation) as it was demonstrated by the tomography scans (Fig. 5B) and by the sequential fluorochrome injection (Fig. 6G). Osteo-PTMC PSIs were in direct contact with the bone tissues of the infraorbital rim and floor, providing an excellent implant osseointegration and physical anchorage. We cannot exclude that mechanobiology did not arbitrate the osteogenesis as well. It is well known that bone repair is sensitive to mechanical factors, which has been widely described in fractured long-bones which heal through endochondral ossification by promoting cartilage callus formation [55]. Importantly, elastic deformation is beneficial and enable better bone formation, whereas shielding the bone defect site from any mechanical loading has been shown to be

detrimental for endochondral and intramembranous bone regeneration [56]. From existing mechanical comparison [25], we can approximate that the titanium implant used in our experimental model (0.4 mm thick) is almost 20 times stiffer than a human OF. Minimizing titanium implant stiffness has been reported to beneficially promote bone regeneration [56], and we cannot exclude that the lower stiffness of Osteo-PTMC *versus* titanium (Fig. 2B) influenced the osseointegration cascade as well. Nevertheless, further studies should be conducted to optimize mechanical properties of implants and investigate the influence of this variable on intramembranous OF healing.

PTMC biodegradation was not observed during the 3-month implantation period. Nevertheless, previous reports have shown that PTMC-based photocrosslinked biomaterials degrade *in vivo* through a surface-erosion mechanism [23], driven by enzymes such as lipases and cholesterol esterases [21,57,58]. This process is clearly different from the common poly(α-hydroxyacids) implants, which degrade through bulk hydrolysis, resulting in a release of acidic oligomers and a sudden and uncontrolled loss of implants mechanical stability [59]. The slow surface erosion of PTMC-based materials allows for creeping substitution of the materials with neo-formed tissue, which could be a key property for the tissue integration and osteoinductive activity observed in this study. To summarize, the capacity of the composite PTMC-based resin to be processed using SLA opens the possibility to produce implants with a high degree of personalization, not only in its shape and geometry, but also according to their mechanical requirements. The design of internal and external PSI architecture can be further optimized for mechanical and biological requirements, depending on the orbital characteristics such as the presence or absence of supportive bony rims, positioning of the screws, overlapping implant/bone interfaces, along with automating the best fitting and fixation options.

## 4. Conclusion

Additive manufacturing of implants based on radiographic data of patients requiring surgical operation is changing the landscape of clinical practices. Nevertheless, hand-shaped titanium implants are still the gold-standard to repair bone fracture sites in the craniomaxillofacial region, such as orbital floor fractures. In this study, we developed a complete work-flow involving the virtual design, the surgical planification, the fabrication, the quality control and the post-implantation monitoring of a patient-specific implant made by stereolithography. By the nature of its components (i.e. poly(trimethylene carbonate) and hydroxyapatite), the Osteo-PTMC implants can be manufactured using photo-fabrication based on patient specific radiographic data, are biodegradable and have intrinsic osteoinductive properties. On a large animal study, we demonstrated the benefices of Osteo-PTMC compared to standard titanium mesh to regenerate the orbital floor. These qualities make Osteo-PTMC a promising synthetic bone graft substitute as an alternative to titanium implants, which is printable and with an unprecedented translational potential in craniomaxillofacial surgery where precise anatomical reconstruction is necessary. Further studies are required to validate the benefice of mechanically-tailorable PSI to enhance the bone regeneration of such defects.

## 5. Experimental section

### 5.1. Design of the PSI

Following pre-operative CT scans (SOMATOM Emotion 6, Siemens Healthcare GmbH, Erlangen, Germany) of the right orbital area of the sheep (n = 12), the region of the OF to be reconstructed with the implant was delineated manually using landmarks. These landmarks were triangulated and processed resulting in a surface covering the region of interest (ROI) with 0 thickness. The thickness or PSI desired profile was achieved by duplicating and translating each triangle along its normal vector. The resulting surfaces were merged and the sidewall, connecting the two extremity parts, was generated. Finally, the implant was smoothed and re-meshed to achieve highly regular triangularization.

Designed models of implants and cylinders (for intra-muscular implantation, IM) with a gyroid-shaped porosity were prepared using K3DSurf (Abderrahman Taha, http://k3dsurf.sourceforge.net/) and Rhinoceros® 4 software (Robert McNeel & Associates). A description of the preparation of these models is given SD 1.

### 5.2. SLA-production of composite implants

Virtual models were sliced into 50 μm thick layers using the Perfactory® software suite of EnvisionTec. These layers were processed into 3D structures on an EnvisionTec Perfactory3® SXGA + Standard UV stereolithograph, using photo-curable resins and irradiation times of 9 s per layer at 180 mW/dm$^2$. Two photo-curable resins were prepared, based on three-armed, methacrylate end-group functionalized poly (trimethylene carbonate) (PTMC-MA) and nano-hydroxyapatite (HA, needle-like HA crystals kindly provided by Xpand Biotechnology BV (Bilthoven, The Netherlands)) and were processed for stereolithography as described in previous works [24,60]. The resin composition was adjusted in order to fabricate structures without HA and with 40 wt% HA (structures called PTMC and Osteo-PTMC respectively). A detailed composition of these resins is given in SD Table 2.

Following SLA-fabrication, the structures were extracted in a mixture of propylene carbonate and ethanol (50% (v/v) each) for three days while refreshing the extraction medium daily. Residual propylene carbonate was thereafter extracted by reducing the propylene carbonate content of the extraction mixture to 0% in a stepwise manner. Finally, the extracted structures were dried at ambient conditions until constant weight and sterilized using cold ethylene oxide gas and degassed for 5 days.

### 5.3. Design optimization, control and characterization of the PSIs

In order to investigate the structural reinforcement effect of the cross-shaped region, finite element (FE) models of the PSI having a gyroid porous structure with and without the internal reinforcing structure were created from the STL files. The surface geometries of the two PSI design models were co-registered into the same coordinate system using Amira™ 6.0.0 (Amira, FEI Company, Hillsboro, Oregon, United States of America) and imported into ScanIP M-2017.06 (Simpleware Ltd., Exeter, UK). The models were meshed with quadratic tetrahedral elements (C3D10) using the following settings of ScanIP: target minimum edge length of 0.1 mm, maximum edge length of 0.275 mm, target maximum error of 0.005 mm, surface change rate of 50; volumetric change rate of 30. The resulting number of elements was approximately 780′000 with a mean edge length of 0.2 mm and the number of nodes was approximately 1.3 million. The material properties were assumed to be homogeneous, isotropic and linear elastic. According to the previously characterized properties of Osteo-PTMC [60], Youngs modulus was set to 60 MPa and a Poisson ratio of 0.3 was used. The models were imported in Abaqus 6.13-3 (Simulia™, Dassault Systemes, Velizy-Villacoublay, France). Loading conditions were defined to mimic the cantilever bending setup used in the experimental mechanical test, later described. The displacement of the fixation region corresponding to the fish-tail-shaped part of the implant was constrained in all directions. Loading was simulated with a 0.3 N vertical force distributed homogeneously in a 4 mm diameter circular region, center of which was located at a 10 mm distance from the fish-tail-shaped part. The FE analyses were performed in the standard implicit solver of Abaqus and the average displacement of the loaded circular region was extracted. Structural stiffness was evaluated as the applied load divided by the resulting displacement. The versatility of the PSI design envelop was also demonstrated by varying the pore sizes and shapes and by developing other reinforcement structures (SD 2).

As a proof-of-concept, a quality control of SLA-fabricated PSIs was

undertaken using a procedure recently validated by our group [61], to characterize the precision of the SLA technique to produce implants compared to the initial CAD models. First, the CAD file was transformed into DICOM images and imported into the microCT database. Subsequently, SLA-fabricated scaffolds were scanned with a cabinet cone-beam microCT (μCT100, SCANCO Medical AG, Switzerland) with the X-ray tube operated at 70 kVp/57 μA, 300 ms acquisition time, 1000 projections/360°. Two-dimensional CT images were reconstructed into 2048 × 2048 pixels matrices with 24 μm nominal resolution. The data was Gaussian-filtered (σ = 0.5, support = 1) to reduce noise. The scaffolds were then segmented using a material specific threshold of 1.28 $cm^{-1}$. The segmented images were co-registered with the CAD model, using 3D rigid registration (using a Powell minimization method of the image correlation function, with tolerance of 0.0001). The aligned images were subtracted, and the differences were used to compute the object correlations (open-pore structure). To estimate matching of the overall volume of the implants, the segmented images were closed using a dilation/erosion of 0.5 mm and the closed objects were registered and aligned using the same technique (close-pore structure). Image processing was performed with EasyIPL a high-level library of macros using the scanner software (IPL).

Mechanical deformation of the PSI fixed at the fish-tail part and titanium implants was performed on a cantilever set-up using an Instron 5866 electromechanical universal testing machine fitted with 10 N load cell. Static loading force of 0.3 N, corresponding to 30 g, which is the average weight of human orbital content [25], was applied at a distance of 10 mm away from the fixation part on both PSI (n = 4) and titanium implants (n = 6) and the degree of bending was continuously registered during 60 min.

### 5.4. Surgical procedure and post-operative follow-up

The preclinical study was conducted in an AAALAC approved facility and according to the Swiss animal welfare act and ordinances (Ethical permission GR 34_2016). Twelve females, skeletally mature (2–4 years old), Swiss White Alpine sheep (69 ± 16 kg) were enrolled in this study. Due to high specimen variability regarding the surface of the OF to be covered by the implants, the 12 sheep were pooled in the two distinct groups (PSI made of Osteo-PTMC or pre-shaped titanium mesh) in a way that the average surface of the materials to be implanted was not significantly different. Prior to the surgery, the animals were acclimatized for 2 weeks (daily cycles of 12 h light/dark) and were fed twice per day with hay, a mineral lick, and hand-fed grain to gain familiarity with caregivers. A veterinarian ensured the sheep to be in good health based on a complete physical assessment and blood analysis (white blood cell count, total protein and hematocrit).

The global work-flow of the animal experiment is shown Fig. 1, and the anesthesia procedure and pain management are reported in SD Table 3. At the day of the surgery, the sheep were placed in lateral recumbency with the right side up. The periorbital area was clipped and carefully cleaned (diluted betadine solution and saline). The eyelids were temporarily closed (ford interlocking suture) and the periorbital area prepared for aseptic surgery with again betadine solution/soap and saline. A skin incision was made from the medial to the lateral canthus, along the processus temporalis. The M. cutaneus faciei and the insertion tendon of the M. malaris were transected and the periosteum carefully lifted to gain access to the lacrimal bulla. The orbital content was then pushed dorsally with a retractor and a Pean forceps was used to create the OF defect. The OF defect was then either reconstructed with a PSI made of Osteo-PTMC (n = 6) or with a preshaped titanium mesh (n = 6, Orbital Floor Mesh Plate 1.3 from DePuy Synthes). As already published, the Osteo-PTMC as a pore diameter of 720 μm and of volume of porosity close to 70% (not including the fish tail and the reinforced cross structure) [24]. The titanium meshes are composed of filaments of with rectangle/trapezoidal shaped pores of 6.3 $mm^2$ in average (SD 3). Both types of implant were secured with 2 titanium 1.5 mm microscrews on the infraorbital rim (on the fish-tail part for the Osteo-PTMC). The incision was then closed in 2–3 layers (periost/subcutaneous tissue Monocryl 4-0) and skin. Then the temporary sutures closing the eye-lids were removed.

In order to assess the potential osteoinductive property of the Osteo-PTMC implants, ectopic-site implantation was also performed intramuscularly (IM). Biomaterials scaffolds 6 mm in height x 9 mm Ø (Osteo-PTMC, PTMC and osteoinductive Ceramic, provided by Xpand Biotechnology BV, Bilthoven, NL)) was implanted through stab incision in the trapecius muscle of every sheep (1 sample per group per sheep). Then, the muscle pocket was sutured with non-absorbable suture to mark the position and the skin was closed (Monocryl 3-0). PTMC was selected as negative control as previous experiment validated its lack of osteoconductivity and a bone forming capability equivalent to an empty defect (in orthotopic site) [24]. Ceramic plugs were used as positive control due to their reported osteoinductivity in previous publication, with similar bone-forming capacity as autologous grafts (in ectopic site) [26].

Post-operatively the sheep wore a head collar with special padding to protect the wound for up to 10 days. The sheep were kept in small groups of 2–3 after the surgery as described above. The animals were routinely checked by a veterinarian or an experienced animal caretaker for general behaviour, body temperature, wound inflammation, respiration, appetite and defecation. Special emphasis was given on bulbus movement or position.

Post-operative clinical CT scans (SOMATOM Emotion 6, Siemens Healthcare GmbH, Erlangen, Germany) of the orbital region of each sheep were performed, just after the surgery, after 4 and 8 weeks under general anesthesia and after euthanasia, 12 weeks. CT scans of the orbita were performed at all respective time-points, and the generated DICOM data were imported into Amira™ 6.0.0 for further analysis. To control post-operatively if the implants covered the ROI initially defined pre-operatively, pre-operative and post-operative CT images were registered using a normalized and iterative mutual information-based image registration procedure allowing rigid motion. Then, the ROI and the region of the implant where overlaid. To verify the implant stability in the OF region over time, the position changes from the first (post-operative) to the last time-point (12 weeks) of the segmented implants was measured point-based and color-coded on the surface of the first time-point. To assess eye displacement over time, the eye position was compared at all time-points with the pre-operative scan and the position change in the dorso-ventral direction was analyzed. For this purpose, the center of the eye was determined by fitting a circle in a plane parallel to the aperture of the orbit. In addition, the repetitive CT scans mentioned above allowed for appreciating the incremental bone deposition, visualized by the increased radiodensity of the implant. The first scan served as a baseline and all subsequent scans were registered to this one. The implants were semi-automatically segmented and their volume including the new ingrown bone was analyzed threshold based. Due to the strong artefact signal given by the metal, such analysis was not possible on titanium implants. The presence of bone ingrowth for the titanium mesh group was consequently assessed post-mortem using a prototype cabinet cone-beam microCT, as described in the next part. Bone healing kinetic was assessed by injection of fluorochromes after 4 weeks (Calcein Green, 10 mg/kg BW SC) and 8 weeks (Xylenol Orange, 90 mg/kg BW SC).

### 5.5. Post-euthanasia sample analysis

12 weeks post-operatively, the sheep were euthanized by 20 mL pentobarbital IV injection. Then the area of the OF was carefully excised, scanned with using high-resolution peripheral quantitative computed tomography (HR-pQCT, SCANCO Medical AG, Switzerland) and stored in 70% methanol until further processing for histology. A titanium-containing explant was scanned using a prototype cabinet cone-beam microCT fitted with a specific filter to alleviate the metal

artefact (μCT100 HE, SCANCO Medical AG, Switzerland) with the X-ray tube operated at 130 kVp, 300 μA, 350 ms acquisition time, 3000 projections/360°. Two-dimensional CT images were reconstructed into 3720 × 3720 pixels matrices with 26 μm nominal resolution. The scaffolds implanted IM were also excised, scanned (microCT 40; 30 μm voxel size, SCANCO Medical AG, Switzerland) and stored in 70% methanol for histological evaluation. Histological evaluation of undecalcified sections were obtained after methylmethacrylate embedding and stained using Giemsa-Eosin as already reported [24].

### 5.6. Statistical analyses

Statistical analysis of data was performed using Prism software (GraphPad Software, La Jolla, CA, USA). We assumed normal distribution of data. One-way ANOVA with Tukey's multiple comparison test was applied to detect significant differences between experimental groups (with $p < 0.05$). Data presented are means ± standard deviation (SD) unless stated otherwise.

## Acknowledgments

The authors would like to acknowledge the National Natural Science Foundation of China, NSFC-DG-RTD Joint Scheme, project No. 51361130034, and the European Union's 7th Framework Program under grant agreement n NMP3-SL-2013-604517, project RAPIDOS, for financial support. Additionally, we are grateful to Eberli, U., Nehrbass D. and Goudsouzian N. for technical and histological assistance. Furthermore, the authors express their gratitude to Prof. J.D. de Bruijn and Dr. Davide Barbieri in Xpand Biotechnology BV for supplying hydroxyapatite nanoparticles.

## Appendix A. Supplementary data

Supplementary data to this article can be found online at https://doi.org/10.1016/j.biomaterials.2019.119721.

## Data availability

The raw data required to reproduce these findings are available to download from https://data.mendeley.com/datasets/cj9cbs3ffw/draft?a=92c69336-3082-497d-a54b-45de13b5b239.

## References

[1] M.A. Geven, V. Varjas, L. Kamer, X. Wang, J. Peng, D. Eglin, D.W. Grijpma, Fabrication of patient specific composite orbital floor implants by stereolithography, Polym. Adv. Technol. 26 (12) (2015) 1433–1438.
[2] J.T. Lichtenstein, A.N. Zeller, J. Lemound, T.E. Lichtenstein, M. Rana, N.-C. Gellrich, M.E. Wagner, 3D-Printed simulation device for orbital surgery, J. Surg. Educ. 74 (1) (2017) 2–8.
[3] C.G.T. Lim, D.I. Campbell, D.M. Clucas, Rapid prototyping technology in orbital floor reconstruction: application in three patients, Craniomaxillofacial Trauma Reconstr. 7 (2) (2014) 143–146.
[4] D.J. Podolsky, J.G. Mainprize, G.P. Edwards, O.M. Antonyshyn, Patient-specific orbital implants: development and implementation of technology for more accurate orbital reconstruction, J. Craniofac. Surg. 27 (1) (2016) 131–133.
[5] R. Grunert, M. Wagner, C. Rotsch, H. Essig, S. Posern, F. Pabst, W.-G. Drossel, J. Lichtenstein, Concept of patient-specific shape memory implants for the treatment of orbital floor fractures, Oral Maxillofac. Surg. 21 (2) (2017) 179–185.
[6] Y.C. Kim, W.S. Jeong, T.-k. Park, J.W. Choi, K.S. Koh, T.S. Oh, The accuracy of patient specific implant prebented with 3D-printed rapid prototype model for orbital wall reconstruction, J. Cranio-Maxillofacial Surg. 45 (6) (2017) 928–936.
[7] M. Kozakiewicz, M. Elgalal, P. Loba, P. Komuński, P. Arkuszewski, A. Broniarczyk-Loba, L. Stefańczyk, Clinical application of 3D pre-bent titanium implants for orbital floor fractures, J. Cranio-Maxillofacial Surg. 37 (4) (2009) 229–234.
[8] K.M. Lee, J.U. Park, S.T. Kwon, S.W. Kim, E.C. Jeong, Three-dimensional pre-bent titanium implant for concomitant orbital floor and medial wall fractures in an east asian population, Archives of Plastic Surgery 41 (5) (2014) 480–485.
[9] U. Vignesh, D. Mehrotra, Dichen, V. Anand, D. Howlader, Three dimensional reconstruction of late post traumatic orbital wall defects by customized implants using CAD-CAM, 3D stereolithographic models: a case report, J Oral Biol Craniofac Res 7 (3) (2017) 212–218.
[10] P. Stoor, A. Suomalainen, C. Lindqvist, K. Mesimaki, D. Danielsson, A. Westermark, R.K. Kontio, Rapid prototyped patient specific implants for reconstruction of orbital wall defects, J. Cranio-Maxillo-Fac. Surg. 42 (8) (2014) 1644–1649.
[11] S.Z. Tabakovic, V.S. Konstantinovic, R. Radosavljevic, D. Movrin, M. Hadzistevic, N. Hatab, Application of computer-aided designing and rapid prototyping technologies in reconstruction of blowout fractures of the orbital floor, J. Craniofac. Surg. 26 (5) (2015) 1558–1563.
[12] T. Kanno, M. Karino, A. Yoshino, T. Koike, T. Ide, H. Tatsumi, K. Tsunematsu, H. Yoshimatsu, J. Sekine, Feasibility of single folded unsintered hydroxyapatite particles/poly-L-lactide composite sheet in combined orbital floor and medial wall fracture reconstruction, J. Hard Tissue Biol. 26 (2) (2017) 237–244.
[13] M. Vehmeijer, M. van Eijnatten, N. Liberton, J. Wolff, A novel method of orbital floor reconstruction using virtual planning, 3-dimensional printing, and autologous bone, J. Oral Maxillofac. Surg. 74 (8) (2016) 1608–1612.
[14] B. Arbez, J.D. Kun-Darbois, T. Convert, B. Guillaume, P. Mercier, L. Hubert, D. Chappard, Biomaterial granules used for filling bone defects constitute 3D scaffolds: porosity, microarchitecture and molecular composition analyzed by microCT and Raman microspectroscopy, J. Biomed. Mater. Res. B Appl. Biomater. 107 (2) (2019) 415–423.
[15] A. Berberi, A. Samarani, N. Nader, Z. Noujeim, M. Dagher, W. Kanj, R. Mearawi, Z. Salemeh, B. Badran, Physicochemical characteristics of bone substitutes used in oral surgery in comparison to autogenous bone, BioMed Res. Int. 2014 (2014) 320790.
[16] D. de Melo Pereira, P. Habibovic, Biomineralization-inspired material design for bone regeneration, Adv. Healthc. Mater. 7 (22) (2018) e1800700.
[17] D. Barbieri, A.J. Renard, J.D. de Bruijn, H. Yuan, Heterotopic bone formation by nano-apatite containing poly(D,L-lactide) composites, Eur. Cells Mater. 19 (2010) 252–261.
[18] D. Barbieri, H. Yuan, X. Luo, S. Fare, D.W. Grijpma, J.D. de Bruijn, Influence of polymer molecular weight in osteoinductive composites for bone tissue regeneration, Acta Biomater. 9 (12) (2013) 9401–9413.
[19] A.A. Ignatius, O. Betz, P. Augat, L.E. Claes, In vivo investigations on composites made of resorbable ceramics and poly(lactide) used as bone graft substitutes, J. Biomed. Mater. Res. 58 (6) (2001) 701–709.
[20] A.C. van Leeuwen, H. Yuan, G. Passanisi, J.W. van der Meer, J.D. de Bruijn, T.G. van Kooten, D.W. Grijpma, R.R. Bos, Poly(trimethylene carbonate) and biphasic calcium phosphate composites for orbital floor reconstruction: a feasibility study in sheep, Eur. Cells Mater. 27 (2014) 81–96 discussion 96-7.
[21] E. Bat, T.G. van Kooten, J. Feijen, D.W. Grijpma, Resorbable elastomeric networks prepared by photocrosslinking of high-molecular-weight poly(trimethylene carbonate) with photoinitiators and poly(trimethylene carbonate) macromers as crosslinking aids, Acta Biomater. 7 (5) (2011) 1939–1948.
[22] K. Fukushima, Poly(trimethylene carbonate)-based polymers engineered for biodegradable functional biomaterials, Biomater Sci 4 (1) (2016) 9–24.
[23] J.J. Rongen, B. van Bochove, G. Hannink, D.W. Grijpma, P. Buma, Degradation behavior of, and tissue response to photo-crosslinked poly(trimethylene carbonate) networks, J. Biomed. Mater. Res. A 104 (11) (2016) 2823–2832.
[24] O. Guillaume, M.A. Geven, C.M. Sprecher, V.A. Stadelmann, D.W. Grijpma, T.T. Tang, L. Qin, Y. Lai, M. Alini, J.D. de Bruijn, H. Yuan, R.G. Richards, D. Eglin, Surface-enrichment with hydroxyapatite nanoparticles in stereolithography-fabricated composite polymer scaffolds promotes bone repair, Acta Biomater. 54 (2017) 386–398.
[25] F. Birkenfeld, E. Behrens, M. Kern, V. Gassling, J. Wiltfang, Mechanical properties of collagen membranes: are they sufficient for orbital floor reconstructions? J. Cranio-Maxillo-Fac. Surg. 43 (2) (2015) 260–263.
[26] H.P. Yuan, H. Fernandes, P. Habibovic, J. de Boer, A.M.C. Barradas, A. de Ruiter, W.R. Walsh, C.A. van Blitterswijk, J.D. de Bruijn, Osteoinductive ceramics as a synthetic alternative to autologous bone grafting, P Natl Acad Sci USA 107 (31) (2010) 13614–13619.
[27] K.K. VanKoevering, D.A. Zopf, S.J. Hollister, Tissue engineering and 3-dimensional modeling for facial reconstruction, Facial Plast Surg Clin North Am 27 (1) (2019) 151–161.
[28] T. Gander, H. Essig, P. Metzler, D. Lindhorst, L. Dubois, M. Rücker, P. Schumann, Patient specific implants (PSI) in reconstruction of orbital floor and wall fractures, J. Cranio-Maxillofacial Surg. 43 (1) (2015) 126–130.
[29] L.M. Ricles, J.C. Coburn, M. Di Prima, S.S. Oh, Regulating 3D-printed medical products, Sci. Transl. Med. 10 (461) (2018).
[30] S. Bose, S. Vahabzadeh, A. Bandyopadhyay, Bone tissue engineering using 3D printing, Mater. Today 16 (12) (2013) 496–504.
[31] F.P. Melchels, J. Feijen, D.W. Grijpma, A poly(D,L-lactide) resin for the preparation of tissue engineering scaffolds by stereolithography, Biomaterials 30 (23–24) (2009) 3801–3809.
[32] R. Ewers, K. Schicho, G. Undt, F. Wanschitz, M. Truppe, R. Seemann, A. Wagner, Basic research and 12 years of clinical experience in computer-assisted navigation technology: a review, Int. J. Oral Maxillofac. Surg. 34 (1) (2005) 1–8.
[33] H. Essig, L. Dressel, M. Rana, M. Rana, H. Kokemueller, M. Ruecker, N.-C. Gellrich, Precision of posttraumatic primary orbital reconstruction using individually bent titanium mesh with and without navigation: a retrospective study, Head Face Med. 9 (1) (2013) 18.
[34] J.W. Shin, J.S. Lim, G. Yoo, J.H. Byeon, An analysis of pure blowout fractures and associated ocular symptoms, J. Craniofac. Surg. 24 (3) (2013) 703–707.
[35] M.J. Chi, M. Ku, K.H. Shin, S. Baek, An analysis of 733 surgically treated blowout fractures, Ophthalmologica 224 (3) (2010) 167–175.
[36] L.H. Hollier, N. Rogers, E. Berzin, S. Stal, Resorbable mesh in the treatment of orbital floor fractures, J. Craniofac. Surg. 12 (3) (2001) 242–246.
[37] R. Kontio, R. Suuronen, Y.T. Konttinen, D. Hallikainen, C. Lindqvist, B. Kommonen,

M. Kellomäki, T. Kylmä, I. Virtanen, P. Laine, Orbital floor reconstruction with poly-l/d-lactide implants: clinical, radiological and immunohistochemical study in sheep, Int. J. Oral Maxillofac. Surg. 33 (4) (2004) 361–368.
[38] B. Sinikovic, F.J. Kramer, G. Swennen, H.T. Lubbers, R. Dempf, Reconstruction of orbital wall defects with calcium phosphate cement: clinical and histological findings in a sheep model, Int. J. Oral Maxillofac. Surg. 36 (1) (2007) 54–61.
[39] L. Koo, M.P. Hatton, P.A. Rubin, When is enophthalmos "significant"? Ophthalmic Plast. Reconstr. Surg. 22 (4) (2006) 274–277.
[40] B.M. Hosal, R.L. Beatty, Diplopia and enophthalmos after surgical repair of blowout fracture, Orbit 21 (1) (2002) 27–33.
[41] J.R. Boyette, J.D. Pemberton, J. Bonilla-Velez, Management of orbital fractures: challenges and solutions, Clin. Ophthalmol. 9 (2015) 2127–2137.
[42] F. Baino, Biomaterials and implants for orbital floor repair, Acta Biomater. 7 (9) (2011) 3248–3266.
[43] F. Baino, S. Perero, S. Ferraris, M. Miola, C. Balagna, E. Verné, C. Vitale-Brovarone, A. Coggiola, D. Dolcino, M. Ferraris, Biomaterials for orbital implants and ocular prostheses: overview and future prospects, Acta Biomater. 10 (3) (2014) 1064–1087.
[44] T.L. Kersey, S.G. Ng, P. Rosser, B. Sloan, R. Hart, Orbital adherence with titanium mesh floor implants: a review of 10 cases, Orbit 32 (1) (2013) 8–11.
[45] H.B. Lee, W.R. Nunery, Orbital adherence syndrome secondary to titanium implant material, Ophthalmic Plast. Reconstr. Surg. 25 (1) (2009) 33–36.
[46] R. de Roche, N. Adolphs, A. Kuhn, S. Gogolewski, B. Hammer, B. Rahn, Rekonstruktion der Orbita mit Polylaktat-Implantaten: tierexperimentelle Ergebnisse nach 12 Monaten und klinischer Ausblick, Mund-, Kiefer-Gesichtschirurgie 5 (1) (2001) 49–56.
[47] S. Uygur, O. Cukurluoglu, S. Ozmen, T.H. Guclu, B. Sezgin, Resorbable mesh plate in the treatment of blow-out fracture might cause gaze restriction, J. Craniofac. Surg. 20 (1) (2009) 71–72.
[48] P. Habibovic, H. Yuan, C.M. van der Valk, G. Meijer, C.A. van Blitterswijk, K. de Groot, 3D microenvironment as essential element for osteoinduction by biomaterials, Biomaterials 26 (17) (2005) 3565–3575.
[49] O. Guillaume, M.A. Geven, D.W. Grijpma, T.T. Tang, L. Qin, Y.X. Lai, H. Yuan, R.G. Richards, D. Eglin, Poly(trimethylene carbonate) and nano-hydroxyapatite porous scaffolds manufactured by stereolithography, Polym. Adv. Technol. 28 (10) (2017) 1219–1225.
[50] Z. Tang, X. Li, Y. Tan, H. Fan, X. Zhang, The material and biological characteristics of osteoinductive calcium phosphate ceramics, Regen Biomater 5 (1) (2018) 43–59.
[51] M. Takemoto, S. Fujibayashi, M. Neo, J. Suzuki, T. Matsushita, T. Kokubo, T. Nakamura, Osteoinductive porous titanium implants: effect of sodium removal by dilute HCl treatment, Biomaterials 27 (13) (2006) 2682–2691.
[52] G.D. Winter, B.J. Simpson, Heterotopic bone formed in a synthetic sponge in the skin of young pigs, Nature 223 (5201) (1969) 88–90.
[53] M. Bohner, R.J. Miron, A proposed mechanism for material-induced heterotopic ossification, Mater. Today 22 (2019) 132–141.
[54] U. Ripamonti, Biomimetic functionalized surfaces and the induction of bone formation, Tissue Eng. A 23 (21–22) (2017) 1197–1209.
[55] E.F. Morgan, K.T. Salisbury Palomares, R.E. Gleason, D.L. Bellin, K.B. Chien, G.U. Unnikrishnan, P.L. Leong, Correlations between local strains and tissue phenotypes in an experimental model of skeletal healing, J. Biomech. 43 (12) (2010) 2418–2424.
[56] A.M. Pobloth, S. Checa, H. Razi, A. Petersen, J.C. Weaver, K. Schmidt-Bleek, M. Windolf, A.A. Tatai, C.P. Roth, K.D. Schaser, G.N. Duda, P. Schwabe, Mechanobiologically optimized 3D titanium-mesh scaffolds enhance bone regeneration in critical segmental defects in sheep, Sci. Transl. Med. 10 (423) (2018).
[57] R. Chapanian, M.Y. Tse, S.C. Pang, B.G. Amsden, The role of oxidation and enzymatic hydrolysis on the in vivo degradation of trimethylene carbonate based photocrosslinkable elastomers, Biomaterials 30 (3) (2009) 295–306.
[58] Z. Zhang, R. Kuijer, S.K. Bulstra, D.W. Grijpma, J. Feijen, The in vivo and in vitro degradation behavior of poly(trimethylene carbonate), Biomaterials 27 (9) (2006) 1741–1748.
[59] M.S. Taylor, A.U. Daniels, K.P. Andriano, J. Heller, Six bioabsorbable polymers: in vitro acute toxicity of accumulated degradation products, J. Appl. Biomater. 5 (2) (1994) 151–157.
[60] M.A. Geven, D. Barbieri, H. Yuan, J.D. de Bruijn, D.W. Grijpma, Preparation and mechanical properties of photo-crosslinked poly(trimethylene carbonate) and nano-hydroxyapatite composites, Clin. Hemorheol. Microcirc. 60 (1) (2015) 3–11.
[61] V.A. Stadelmann, M.A. Geven, D.W. Grijpma, G.R. Richards, D. Eglin, O. Guillaume, Integration of high-resolution micro-computed tomography in the quality control of 3D-printed scaffolds, J. Med. Mater. Technol. (2) (2017) 11-14%V 1.